1-1-1999

Fiber-Spacing Effects in the Solidification Processing of Metal Matrix Composites

M M. Guslick

J E. Simpson

S V. Garimella
Purdue Univ, sureshg@purdue.edu

Numerical Heat Transfer, Part A, 35:587–607, 1999

1040–7782/99 $12.00 + .00

FIBER-SPACING EFFECTS IN THE SOLIDIFICATION PROCESSING OF METAL MATRIX COMPOSITES

Michael M. Guslick, James E. Simpson, and Suresh V. Garimella
Department of Mechanical Engineering, University of Wisconsin–Milwaukee, P.O. Box 784, Milwaukee, Wisconsin 53201, USA

The effects of the presence and packing geometry of reinforcing fibers in a solidifying aluminum matrix are investigated. Particular attention is paid to the effect of changes in the fiber pitch on the thermal field and thus on the propagation of the solidification front. Results of simulations for both low- and high-conductivity (alumina and copper) fibers are presented. For fibers in an in-line configuration, a critical fiber spacing is identified: a fiber pitch smaller than this critical value causes increasing front distortion with each additional fiber that the front passes. When the fiber pitch is at or greater than the critical value, the solidification front has a sufficient distance in which to return to an essentially planar shape. The critical fiber pitch for alumina and copper fibers is approximately 2.5 and 2 fiber diameters, respectively. For staggered fibers, the behavior of the propagating solidification front is more complex, and changes to the critical spacing due to fiber staggering are discussed.

INTRODUCTION

Metal-matrix composites (MMCs) are engineered combinations of a continuous metallic matrix and one or more discontinuous reinforcing phases. The reinforcing phase may be in the form of fibers, whiskers, or particles. Although cast iron and Al-Si alloys—which share features of MMCs—have been in use for many years, modern MMCs offer the advantage of being engineered to conform to a particular set of specifications on weight, stiffness, and wear resistance. In addition, spatial variation in properties may be achieved by modifying the location and composition of the reinforcing material.

A variety of methods for producing MMCs have been developed, including pressure infiltration, die casting, and stir casting. Such methods may be considered liquid-state processes, as the metal matrix is in a molten state at the beginning of the production cycle. Solidification in such liquid-state methods is a complex transformation, and the subtleties of the process need to be understood in order to successfully produce MMCs. Factors such as propagation and stability of the solidifying front in the presence of the reinforcement, movement of the discontinuous phase (fiber/particle pushing and settling), thermochemical reactions at the solidification front, and interfacial bonding between the metallic matrix/reinforcement, all affect the properties of the final product. The present work concentrates on investigating the effects of different fiber configurations and properties on front propagation and interface shape.

Received 29 September 1998; accepted 17 November 1998.
Address correspondence to Suresh V. Garimella, Department of Mechanical Engineering, University of Wisconsin–Milwaukee, P.O. Box 784, Milwaukee, WI 53201, USA. E-mail: sureshg@uwm.edu

NOMENCLATURE

A	area
c_p	specific heat at constant pressure
C_{ij}	coefficient matrix in Eq. (2)
D	fiber diameter; reference length
f	volume fraction
h	enthalpy
k	thermal conductivity
L	length of simulation domain
RHS_{ij}	explicit term matrix in Eq. (2)
t	time
T	temperature
V	volume
α	thermal diffusivity
ΔH	enthalpy of freezing
λ	nondimensional temperature $[= c_{pR}(T - T_m)/\Delta H]$
ρ	density
ϕ	nondimensional enthalpy $[= (h - h_m)/\Delta H]$

Subscripts

f	fiber
H	hot wall temperature condition
i	initial condition
i, j	located at i, jth finite volume center
l	liquid
m	at solidification front
R	reference quantity
s	solid

Superscripts

p	iteration count p

Thermal effects during the infiltration of fiber preforms were analyzed by Mortensen et al. [1]. A similarity solution was obtained for the one-dimensional heat conduction equation. The domain of interest was subdivided into subregions containing un-infiltrated fibers, fibers with a liquid metal matrix, and fibers with a solidifying matrix. The rate of infiltration was constant and determined from D'Arcy's law. Appropriate matching conditions were posed at each boundary, and closed-form solutions were obtained for simple cases. The timescale of the analysis was such that "instantaneous" heat transfer to the fibers from the melt was assumed. In the last phase of this work, the analysis was generalized to include multidimensional heat transfer due to nonadiabatic side walls. The analytical expressions developed in this work were validated by experiments performed by Masur et al. [2]. The experimental results exhibited very good agreement for the one-dimensional analysis but less satisfying agreement for the multidimensional case due to a lack of knowledge of the applied thermal boundary condition. Similarity solutions were also obtained for infiltration with a binary eutectic matrix [3].

Such macroscopic analyses are useful for elucidating the bulk behavior during the synthesis of composite materials but do not consider the finer-scale effects of the influence of the fibers on the thermal field and the shape of the propagating solidification front. Khan and Rohatgi [4, 5] investigated the propagation of the solidification front around various fibers numerically, as did Fan et al. [6]. It was demonstrated that the fibers have a strong impact on the shape and progression of the propagating solidification front.

The aim of this paper is to present numerical results for the solidification of a pure aluminum matrix in the presence of low- (alumina) and high-conductivity (copper) fibers, in an in-line and staggered configuration. Solidification will be

normal to the axis of the fibers. The emphasis of this analysis is the influence of fiber configuration on front propagation; the effects of shrinkage, fiber/matrix wetting, and dendritic growth are neglected. The reinforcing fibers are stationary, and the front is considered smooth. Single fibers [7] and in-line, multiple fibers in pure-metal and alloy matrices [8] have been considered previously. It will be seen from the present work that in addition to the fiber properties, the fiber configuration (staggered or nonstaggered) and the spacing between the fibers (fiber pitch) have a significant impact on the resulting thermal field and hence the propagation of the solidification front. In particular, it will be seen that certain configurations favor an interface shape which is not significantly distorted as it impinges upon each fiber, whereas other configurations lead to the formation of a distorted front (which becomes increasingly more distorted as solidification progresses). In this latter case, the fibers may be pushed out of regular alignment, which would be detrimental to the properties of the final product.

MATHEMATICAL FORMULATION AND NUMERICAL ANALYSIS

The solution scheme used in this work and its performance in validation problems are explained in full detail elsewhere [7]; salient details are provided here. Figure 1*a* shows a closed two-dimensional rectangular cavity with three adiabatic walls and a single cold wall at the left held at a constant temperature T_c. A solidifying metal initially at a superheated temperature T_i is contained within the cavity with solid fibers interspersed throughout on a square grid. Planes of symmetry within the domain allow the system to be simplified down to a single section, which repeats identically throughout the cavity. For staggered fibers, the domain is as shown in Figure 1*b*. All energy transport in the system is via conduction; since the volume fraction of fibers for the cases considered in this work ranges from 35 to 79%, the magnitude of convective velocities is expected to be small. Convection effects have therefore been ignored.

The integral form of the law of conservation of energy is

$$\int_t^{t+\Delta t} \frac{\partial}{\partial t}\left(\int_V h\, dV\right) dt = \int_t^{t+\Delta t}\int_A -(k\,\nabla T)\cdot \mathbf{n}\, dA\, dt \tag{1}$$

Equation (1) is solved in nondimensional form; the reference length and time are D and D^2/α_R, respectively, while enthalpy and temperature are nondimensionalized as $\phi = (h - h_m)/\Delta H$ and $\lambda = c_{pR}(T - T_m)/\Delta H$.

The solution scheme to be applied to Eq. (1) is a Gauss-Seidel iteration with successive overrelaxation. Equation (1) becomes

$$\phi_{i,j}^{p+1} + C_{i,j}^{p}\lambda_{i,j}^{p+1} = \mathrm{RHS}_{i,j}^{p} \tag{2}$$

The values at time step n are used as the first approximation to the solution. Convergence is assessed by examining the maximum value of the change in the solution and the magnitude of the residual; convergence is declared only if both of these are below a tolerance of $\varepsilon = 10^{-6}$ [9].

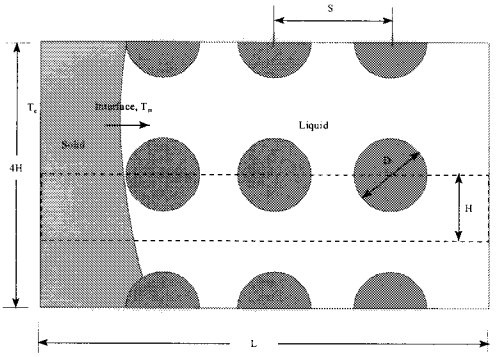

(*a*)

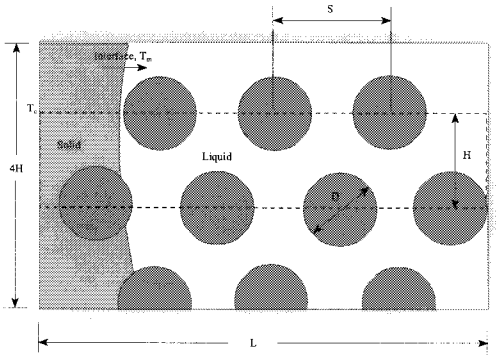

(*b*)

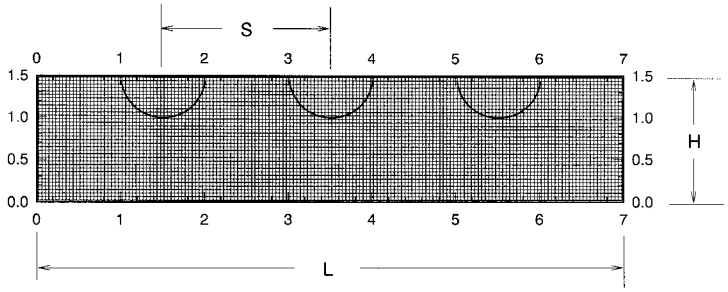

(*c*)

Figure 1. The solidification cavity being investigated with (*a*) in-line fibers and (*b*) staggered fibers. The computational domain, chosen based on symmetry, is shown enclosed by a dashed line. (*c*) A representative computational mesh—the mesh varies based on the fiber spacing, but the cell size is fixed for all cases.

RESULTS

In-Line Fibers

The first set of simulations considered an in-line fiber layout with three 10-μm-diameter fibers as illustrated in Figure 1*a*. The domain height is fixed at 15

μm ($H = 1.5D$), while the domain length ranges from 50 to 90 μm ($L = 5D$–$9D$) as the fiber pitch S is increased. The second set of simulations used a staggered fiber layout as shown in Figure 1*b*, with a total of six fibers in a domain size of 15–35 pm high by 80–130 μm wide. Both alumina and copper fibers were considered in each set of simulations. Copper fibers have been chosen only to illustrate the behavior of the front in the presence of fibers with a high thermal conductivity and low specific heat (in practice, copper fibers would react with aluminum to form intermetallics). This will provide a contrast to the results found with alumina fibers. The domains were discretized with a regular-cell mesh of size 0.4166 μm (a representative mesh is shown in Figure 1*c*) and simulated with a time step of 0.01540 μs. This mesh size and time step were found to be adequate from numerical experiments [7]. The thermophysical properties [5] used are provided in Table 1.

The initial temperature of the molten matrix was set at $T_i = 760^\circ$C, and the cold wall temperature was set at $T_c = 460^\circ$C [5]. The simulations were performed on a HP 715/100 workstation (100 MHz, SPECfp95 3.47) with code written in ANSI standard FORTRAN 77. Computation times varied from 49 to 221 min, depending on fiber properties and domain size.

Figure 2*a* shows the solidification front locations for three touching alumina fibers ($S = D$). The front starts out being nearly vertical when it has not yet interacted with any of the fibers. As the front approaches the first fiber, an increasingly smaller area of liquid remains between the fiber and the upper portion of the solidification front. The alumina fiber has a very low thermal conductivity in comparison with either the solid or liquid aluminum and acts as a nearly adiabatic wall, transferring minimal heat. Since the front location remains nearly normal to adiabatic walls, the front curves toward the fiber as it makes contact, accelerating the front propagation. As the front progresses approximately halfway past the first fiber, the low thermal conductivity of the fiber has a greater effect, retarding the front movement near the fiber. Upon encountering the second fiber, front progression is again accelerated, straightening the front to a nearly vertical condition as it passes the center of the second fiber. Front progression is slowed as it reaches the trailing side of the second fiber. This cycle repeats once more as the front passes the third fiber. As the front finally departs from the third fiber, it is severely curved toward the fiber but begins reverting to vertical as it progresses further, unimpeded by more fibers.

Figure 2*b* shows front locations for $S = 1.5D$. The behavior is similar to that in Figure 2*a* with the front alternately curved forward and then back while progressing past each fiber. However, as the fiber spacing increases (each succes-

Table 1. Thermophysical properties [5] for aluminum matrix and alumina and copper fibers

Property	Aluminum matrix	Alumina fiber	Copper fiber
k_s, W/(m K)	237.65	3.975	401
k_l, W/(m K)	94.14		
c_{ps}, J/(kg K)	903.74	1071.1	385
c_{pl}, J/(kg K)	1079.47		
ρ, kg/m^3	2700	3970	8933
ΔH, kJ/kg	397.48		

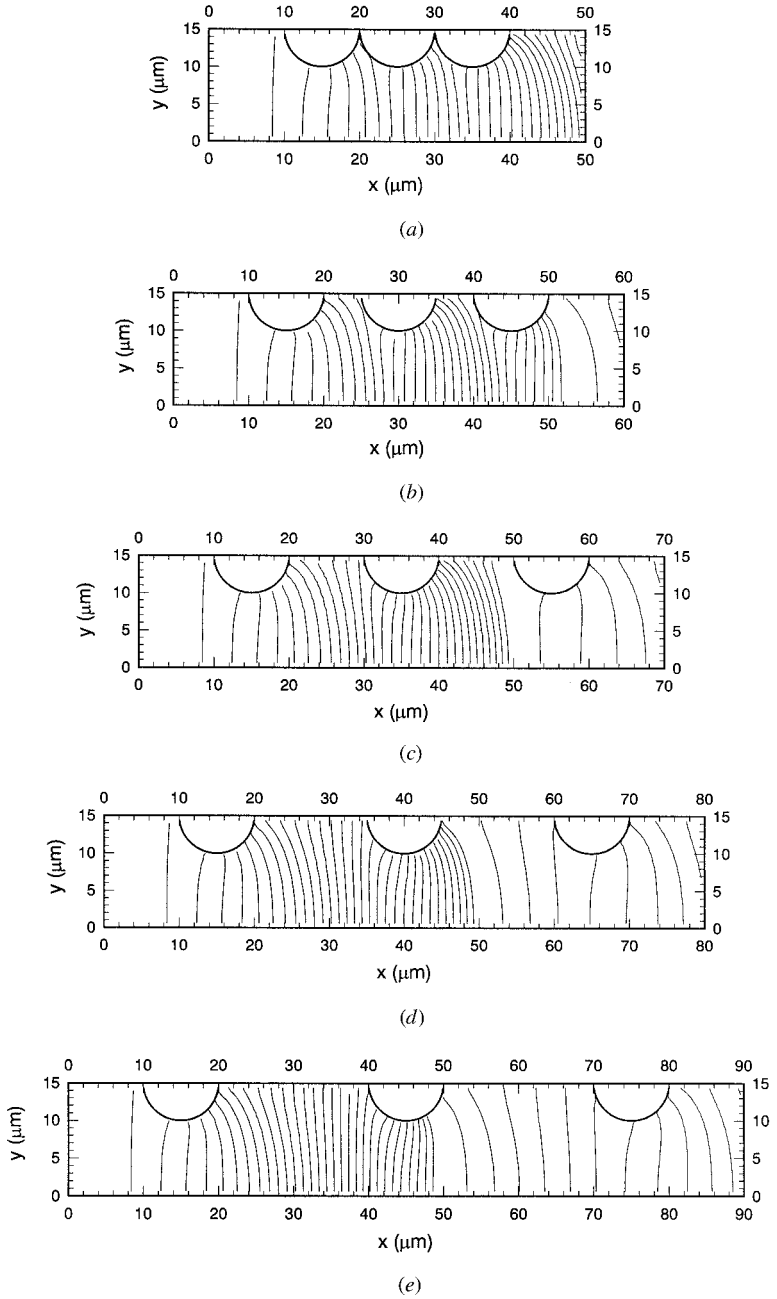

Figure 2. Front locations for aluminum solidification with alumina fibers. An interval of 1.54 μs is used for the first 30 fronts, with an interval of 7.7 μs for all remaining fronts. Fiber pitches used are (*a*) 1, (*b*) 1.5, (*c*) 2, (*d*) 2.5, and (*e*) 3 fiber diameters.

sive figure has a spacing of 1 fiber radius more than the previous figure), the effects of the fiber on the advancing solidification front become smaller. Increased spacing between fibers allows the solidification front to return fully to its original vertical orientation. In Figure 2*c* the solidification front has nearly returned to a vertical orientation upon reaching the second fiber. Any additional spacing beyond a pitch of approximately 2.5 fiber diameters ($S = 2.5D$) has no additional effect, as seen in Figures 2*d* and 2*e*—there is no discernible difference in front curvature upon reaching the second fiber. This behavior is seen again as the front approaches the third fiber; Figures 2*d* and 2*e* show very similar solidification fronts contacting the third fiber.

The influence of copper (high-conductivity) fibers on solidification front progression is illustrated in Figure 3. The effects are even more drastic than for the alumina fibers. In contrast to the behavior with alumina fibers, the front is first decelerated as it approaches the copper fiber. As the front continues to propagate forward, traversing through the fiber, it is accelerated by the fiber, since the high thermal conductivity of the copper draws more heat through than solid aluminum. This continues with each additional fiber, and the front becomes stretched, since the front progression at the bottom of the region is slower. This effect is apparent, for example, in Figure 3*a* at 13.86 μs, when the bottom edge of the solidification front is just past the contact point of the first and second fibers, whereas the upper edge of the front has progressed almost entirely around to the right side of the fiber. As for alumina fibers, the solidification front straightens out after passing all the fibers, returning to near vertical. However, the front returns to a vertical orientation more quickly with the copper fibers. This behavior continues as the fiber pitch is increased. The influence of the copper fibers on front acceleration is shown most strikingly in Figure 3*c* at 38.5 μs. The bottom of the front is approximately 0.5 μm past the third fiber, whereas the top of the front has been accelerated entirely around this fiber. Although difficult to see in the figure, there is, in fact, a very thin layer of solidified aluminum between the front and the fiber.

Not only do the copper fibers result in a local acceleration of the solidification front, but they also lead to more rapid solidification in the entire domain. In Figure 2*a* the domain with alumina fibers has solidified in 43.12 μs. Using copper fibers in the same arrangement, the solidification time is reduced to 29.26 μs, as shown in Figure 3*a*, reflecting a 30% reduction in solidification time. This time difference decreases as the fiber spacing increases. However, at a fiber pitch of 3 diameters, the solidification time with copper fibers is still $\sim$ 20% less than that with alumina fibers.

In comparing the results of simulations for different spacings with either set of fibers, there appears to be a critical fiber spacing that determines whether or not a solidification front will grow more distorted as it encounters additional fibers. At the minimum fiber pitch in Figure 2*a*, the solidification front has not become entirely vertical when it contacts the second or third fibers. In Figure 2*c* the front is nearly vertical upon reaching the second fiber, and in Figure 2*d*, the front has fully returned to vertical when it contacts the second fiber. This behavior is also seen more clearly with copper fibers. In Figure 3*a* the distortion of the front from top to bottom as measured by the x value over which the front stretches (Δx) is roughly 2 μm at 6.16 μs (front at the end of the first fiber); in comparison, at 61.6

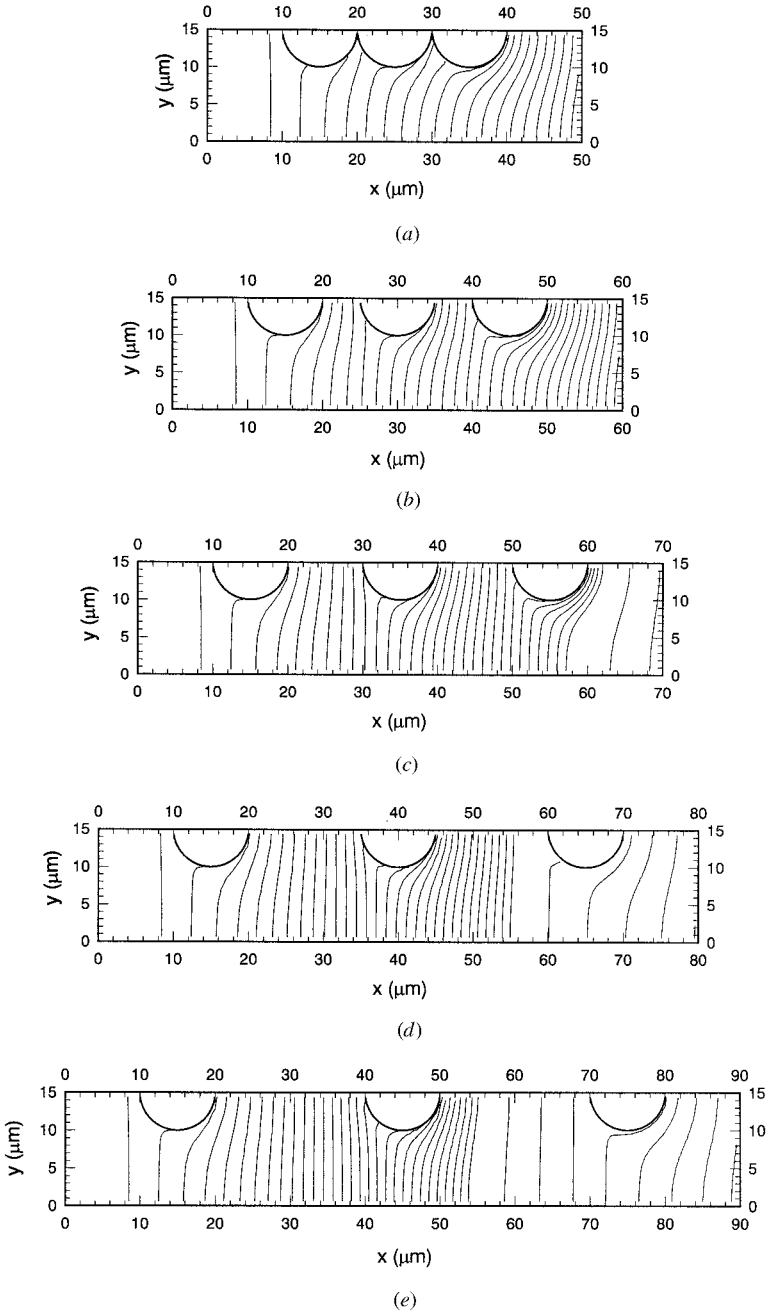

Figure 3. Front locations for aluminum solidification with copper fibers; the times and fiber pitch values are the same as in Figure 2.

μs, when the top of the front has passed the third fiber, the distortion of the front is over $\Delta x \approx 10$ μm. In Figure 3*b* the distortion from additional fibers is considerably less, and in Figure 3*c* the front is able to return to a fully position before encountering additional fibers. These cases show that the *critical pitch* for regularly packed, in-line fibers, S_C, is $\sim 2.5D$ for alumina fibers and $2D$ for copper fibers.

Figure 4 shows the effects of the alumina fibers on the temperature fields in the domain, early in the solidification process (at 4.62 μs), with S varying from $1D$ to $3D$. At $S = D$ (Figure 4*a*), the temperatures experienced in the aluminum matrix over almost half of the domain are bunched much more tightly within the first fiber alone, illustrating the dramatic impact of the low fiber thermal conductivity on the thermal field. This behavior continues as the fiber pitch is increased (Figures 4*b*–4*e*). Figure 5 shows the contrasting effects of copper fibers on the temperature field for the same conditions as in Figure 4. In contrast to the alumina fibers, the copper fibers distort the thermal field by spreading the isotherms apart in the fiber and its vicinity, for all the pitches tested. Note that the distortion in these cases is more localized than for the alumina fibers.

The temperature field toward the end of the solidification process is considered next. The temperature gradient in the solidified part of the domain is, by now, much reduced. With alumina fibers in Figure 6, the isotherms tend to be swept back (as do the front locations) and pinched near the top, where they are influenced by the fibers, while at the bottom, the isotherms are evenly spaced. With copper fibers (Figure 7), the isotherms in the solidified area are less distorted than in Figure 6, despite the fact that the solidification front is significantly more distorted with copper fibers. The isotherm spacing in the copper fibers is slightly greater than in the aluminum matrix. Also, despite the faster progression of the solidification front, the high thermal conductivity of the copper fibers quickly smooths out temperature profiles in the solidified section. In contrast, the alumina cases in Figure 6 show distorted temperature profiles well after the area has solidified.

Staggered Fibers

The next series of simulations examines the effects on the front propagation of staggering the fibers in alternate columns (Figure 1*b*). Instead of having three fibers equally spaced along the top wall of the domain, a total of six fibers must now be considered. The fiber closest to the cold wall is at the top, with successive fibers alternating between the bottom and top (as shown in Figures 8 and 9). In addition to the HP 715 workstation, a Silicon Graphics Indigo 2 (250 MHz, SPECfp92 122.9) was also employed in these calculations. The time step and cell size in the mesh were unchanged. The values of fiber pitch tested were $S = 2$, 3, 4, 6, and $8D$, while the values of transverse spacings (domain heights) tested were $H = 1.5$, 2, 2.5, 3, and $3.5D$. For the staggered fibers the pitch is still defined as the spacing between fiber centers in a given column. This test matrix resulted in a total of 50 simulations being performed. Results are described in detail, and plots are provided for two representative cases: one with $S = 2$, 3, and $4D$ at a fixed transverse spacing of $H = 1.5D$, and another for transverse spacings of $H = 1.5$, 2.5, and $3.5D$ at a fixed pitch of $S = 2D$.

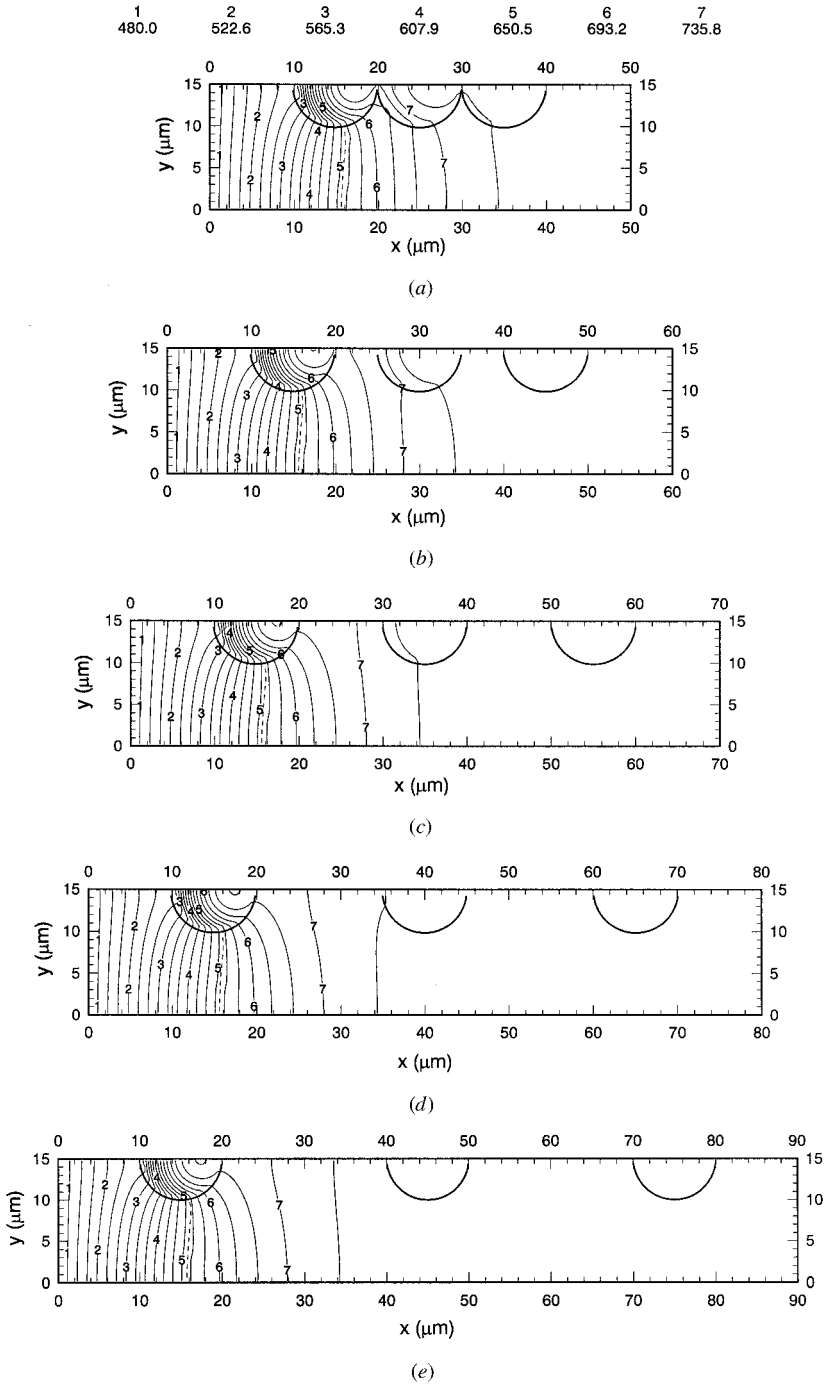

Figure 4. Temperature profiles for aluminum solidification with alumina fibers at 4.62 μs for the pitches considered in Figure 2.

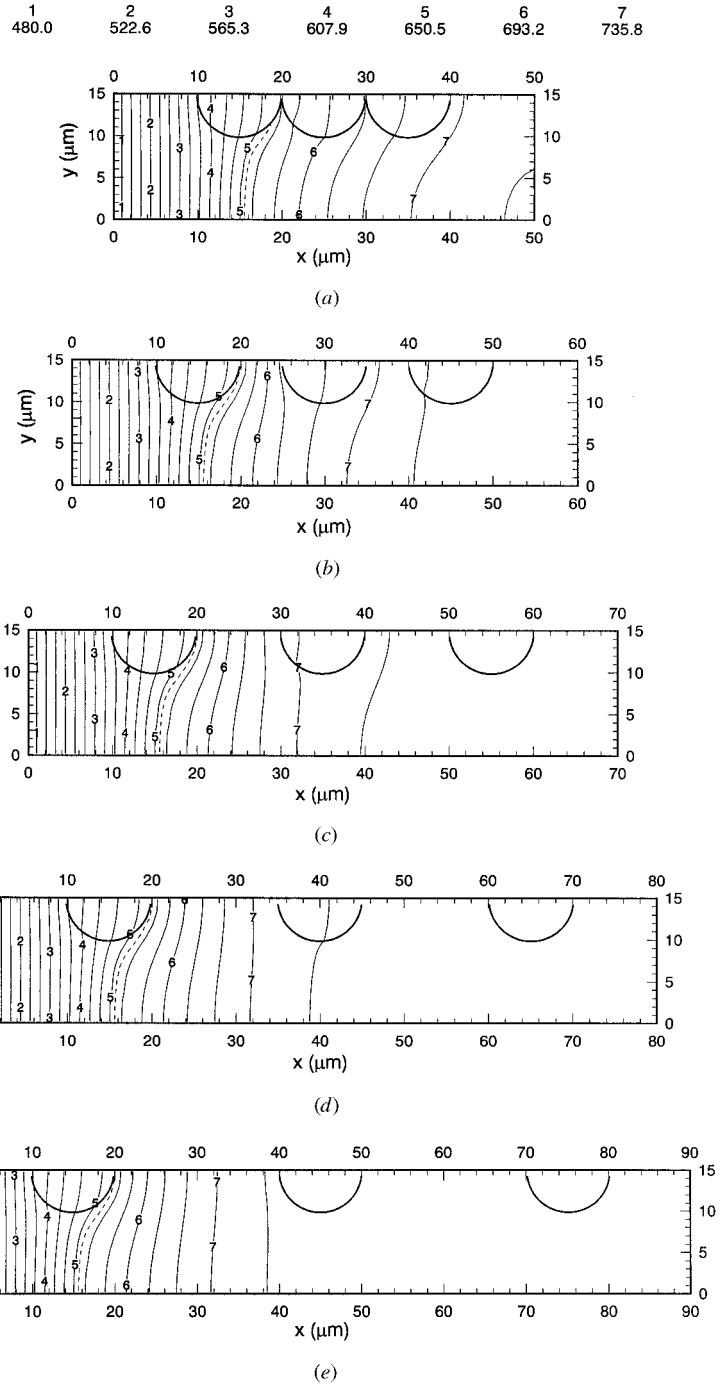

Figure 5. Temperature profiles for aluminum solidification with copper fibers at 4.62 μs for the pitches considered in Figure 2.

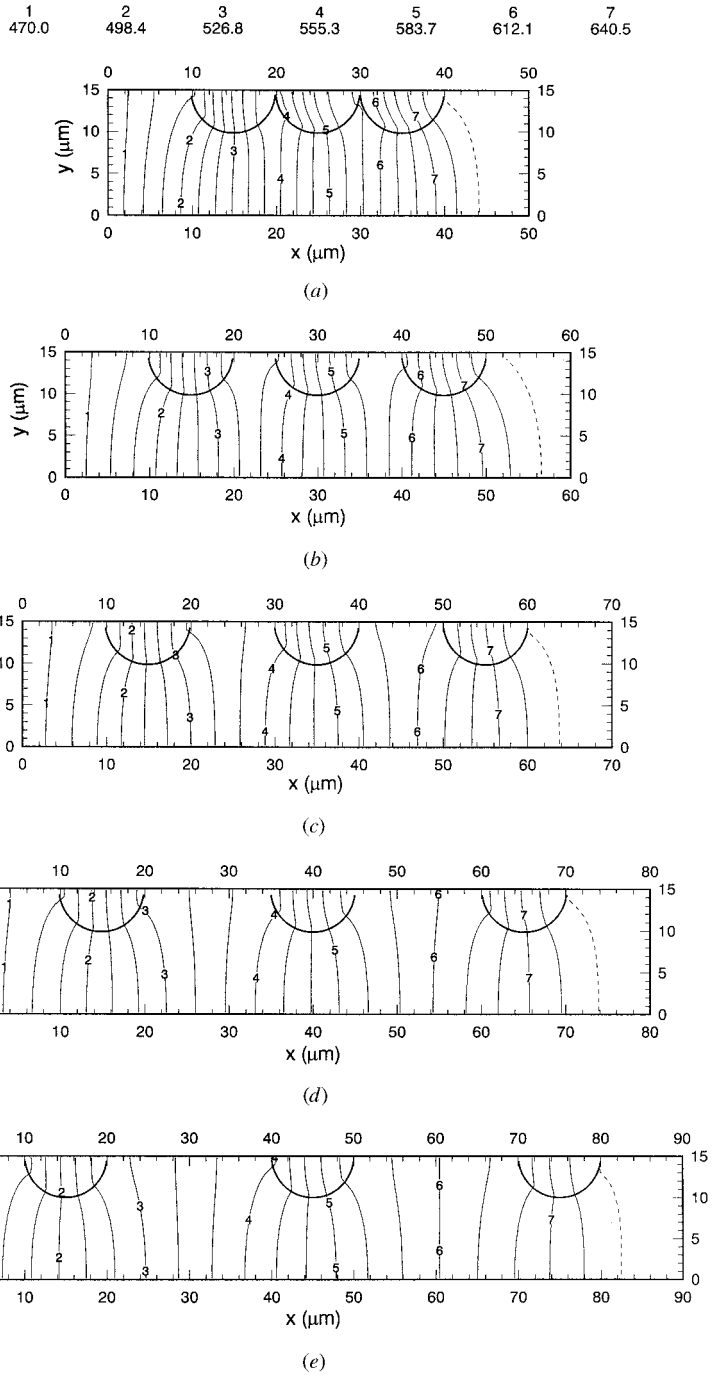

Figure 6. Temperature profiles for aluminum solidification with alumina fibers late in the process: (*a*) $S = 1D$ at 32.34 μs, (*b*) $S = 1.5D$ at 53.9 μs, (*c*) $S = 2D$ at 69.3 μs, (*d*) $S = 2.5D$ at 92.4 μs, and (*e*) $S = 3D$ at 115.5 μs.

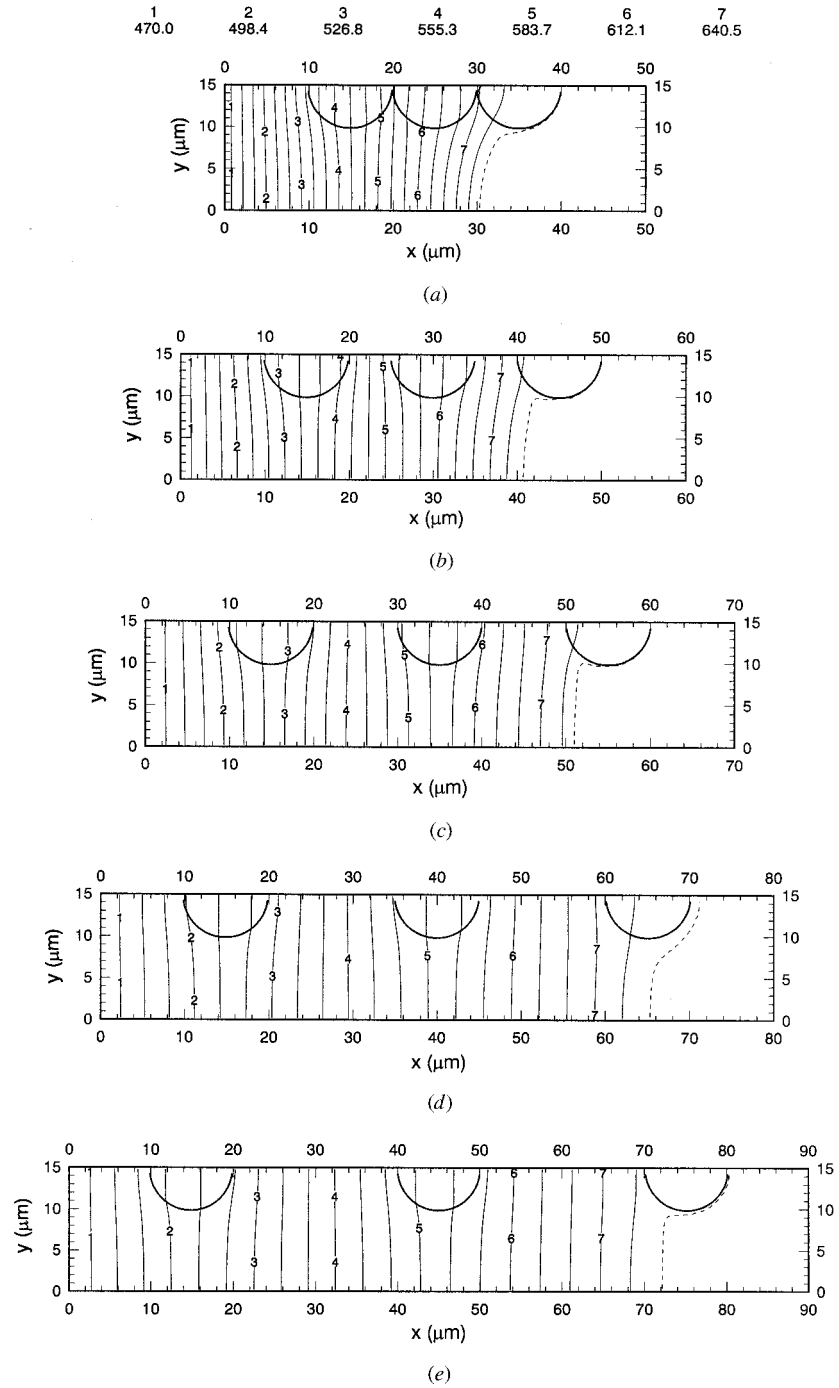

Figure 7. Temperature profiles for aluminum solidification with copper fibers late in the process: (*a*) $S = 1D$ at 13.86 μs, (*b*) $S = 1.5D$ at 24.64 μs, (*c*) $S = 2D$ at 38.5 μs, (*d*) $S = 2.5D$ at 61.6 μs, and (*e*) $S = 3D$ at 77 μs.

With alumina fibers in a staggered layout (Figure 8*a*), there is little difference in the first few front locations as compared to an in-line fiber layout. However, as the solidification front advances toward the second fiber, the front comes under the influence of two fibers simultaneously (Figure 8*a*). This causes a distortion of the front, resulting in its being angled back from the vertical until the front passes the first fiber entirely. The front then quickly straightens toward vertical until it contacts the third fiber. The front is then angled forward, as it is once again under the influence of two fibers simultaneously. This mode of propagation continues, with the front sloping alternately backward and forward. Once past the final fiber, the front propagates as for an in-line arrangement and restores to vertical as the cavity becomes fully solidified. As the pitch is increased (Figure 8*b*), the solidification front is not under the influence of two fibers simultaneously for as long. None of the front locations in this figure is distorted to the same extent as in Figure 8*a*. As the pitch is increased further, the fronts are seen to contact only a single fiber at a time (Figure 8*c*).

Changing the transverse spacing between fibers, which in this study is achieved by stretching the domain vertically, has the effect of decreasing the resistance to front progression when low-conductivity alumina fibers are used. Whereas at a close transverse spacing ($H = 1.5D$, Figure 9*a*) the domain solidified

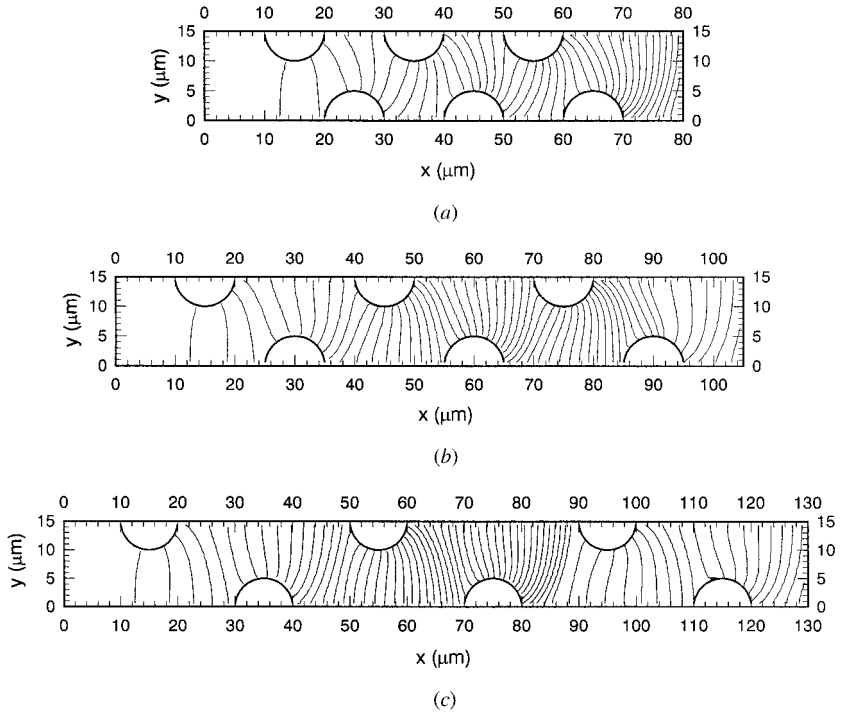

Figure 8. Front locations for aluminum solidification with staggered alumina fibers. An interval of 3.08 μs is used for the first 50 fronts, with an interval of 7.7 μs for all remaining fronts. The transverse fiber spacing is fixed at $H = 1.5D$, with fiber pitches S of (*a*) 2, (*b*) 3, and (*c*) 4 fiber diameters.

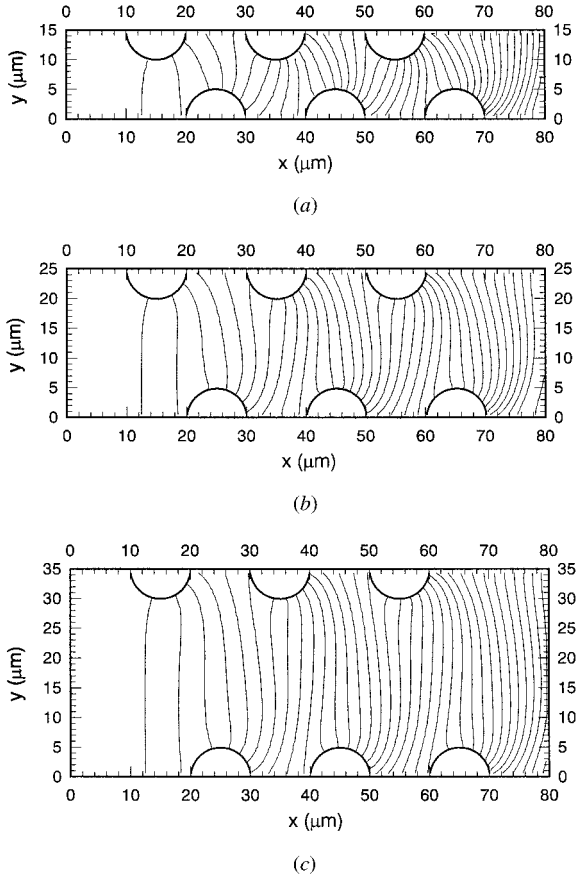

Figure 9. Front locations for aluminum solidification with staggered alumina fibers. The fronts are plotted at the same time intervals as in Figure 8. The fiber pitch is fixed at $S = 2D$ with transverse spacings H of (*a*) 1.5, (*b*) 2.5, and (*c*) 3.5 fiber diameters.

completely in over 123.2 μs, increasing the spacing to $H = 2.5D$ (Figure 9*b*) decreased the total solidification time to roughly 110.9 μs; a further increase in spacing to $3.5D$ decreases this time to 107.8 μs. The larger transverse spacing also allows the solidification fronts to remain more closely vertical than in the constrained conditions of Figure 9*a*. Figure 9*c* shows that the fibers have a limited range of influence on front progression. The fronts are primarily straight, with strong curvature only at the ends where fibers are contacted.

When copper fibers are present in the domain instead of alumina fibers, Figure 10*a* shows that even at the smallest transverse spacing, the solidification front is under the influence of only a single fiber at a time. Due to the high fiber thermal conductivity, by the time the portion of the front that is essentially planar and remote from the fiber has reached the x location of the fiber midpoint, the section of the front near the fiber has already advanced beyond the fiber. The front, however, still exhibits the back and forth sloping seen for alumina fibers,

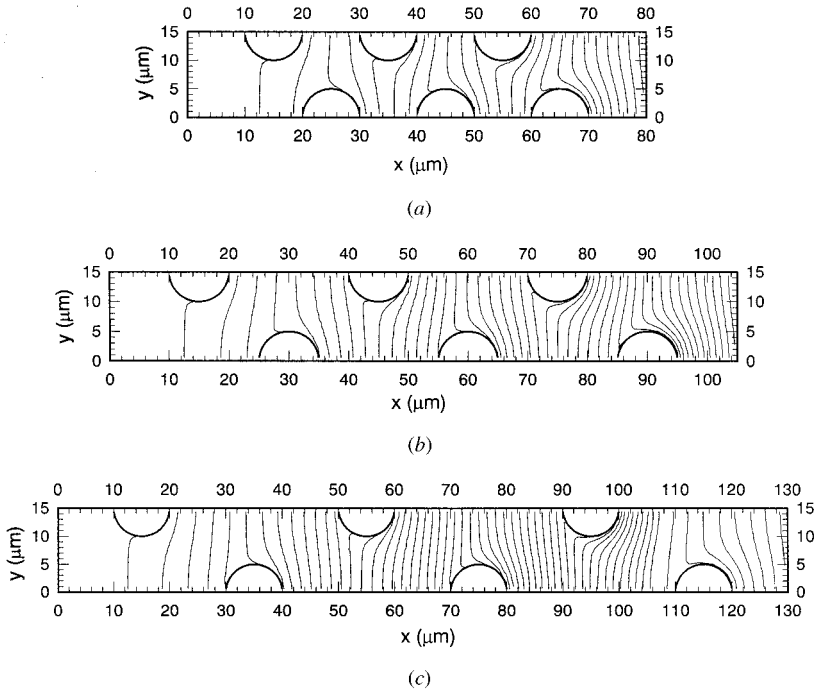

Figure 10. Front locations for aluminum solidification with staggered copper fibers as a function of fiber pitch; remaining details as in Figure 8.

although the effect is less dramatic. Increasing the pitch to $S = 3D$ and $4D$ (Figures 10*b* and 10*c*) has the expected effect of allowing the front more time to relax to vertical. The interactions between the front and staggered copper fibers for large fiber pitches are remarkably similar to those seen for in-line copper fibers of the same pitch.

An increased transverse spacing for staggered copper fibers (Figure 11) leads to a reduced distortion of the front as in Figure 9. However, whereas the increase in transverse spacing caused a decrease in total solidification time with alumina fibers, the higher conductivity of copper fibers causes the solidification time to increase from 64.68, to 80.08, to 83.16 μs for $H = 1.5$, 2.5, and $3.5D$, respectively.

Figures 12 and 13 show thermal fields in the staggered alumina fiber domains near the end of solidification. Like the in-line cases in Figure 6, the alumina fibers have the effect of pinching the isotherms together, even long after a particular area has solidified. Staggering the fibers is seen to sweep the isotherms alternately back and forth, as for the fronts in previous figures. Thermal fields in the staggered copper fiber domains are similar to those seen for in-line fibers in Figure 7, and are not shown.

Consideration of the front propagation in the presence of staggered fibers at varying pitches and transverse spacings, including results not shown here, reveals some complex and interesting phenomena. A summary of the results for front orientation is provided in Table 2. Alumina fibers are considered first. At the smallest spacing tested of $H = 1.5D$, a critical fiber pitch at which the front returns to vertical was not encountered for the pitches investigated. This is due to

the influence of the staggered fiber layout on the thermal field. As the front passes between successive upper fibers, the lower fibers influence its shape sufficiently to prevent it from returning to vertical (planar). At the largest spacings tested of $H = 3D$ and $3.5D$, the fibers behave in a manner identical to the in-line fibers, and the existence of a critical pitch is observed. At a pitch of $S = 2D$, the front is distorted, while increasing the fiber pitch to $S = 3D$ and beyond results in a planar front. This suggests a critical fiber spacing of about $S_C = 2.5D$, as for the in-line case.

At the intermediate transverse spacings of $H = 2D$ and $2.5D$, the solidification front behavior is more complex. At pitches smaller than the in-line critical spacing ($S_C = 2.5D$), the front is distorted. At a larger pitch of $3D$, the front returns to planar between fibers. However, as opposed to the larger transverse spacings ($H \geqslant 3D$), the front again becomes distorted as the pitch is increased further ($S = 4D$ and $5D$ for $H = 2D$, and $S = 4D$ for $H = 2.5D$). Thus, at intermediate H, the front progression lapses from being planar at $S \sim S_C$, to being angled at somewhat larger pitches. As the pitch is increased beyond these interme-

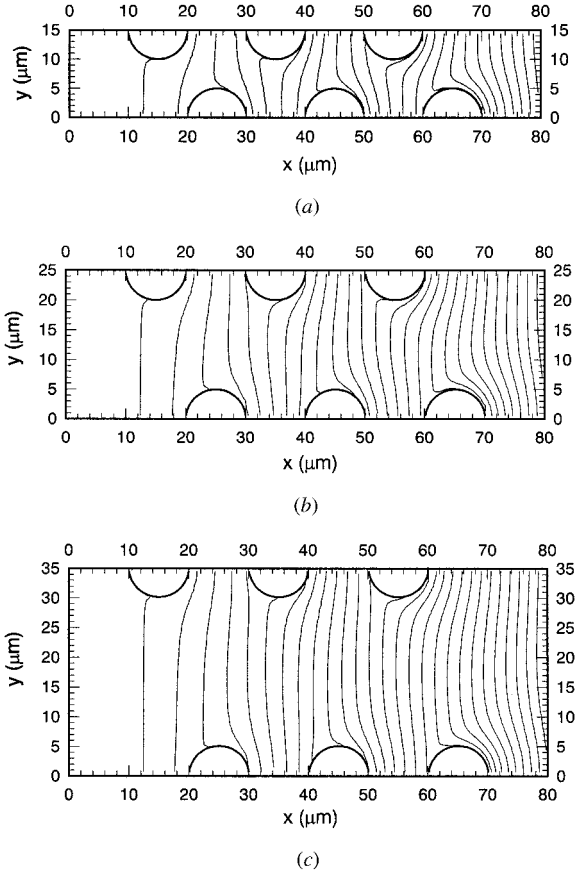

Figure 11. Front locations for aluminum solidification with staggered copper fibers as a function of transverse spacing; remaining details as in Figure 9.

diate values, the front propagation becomes planar once again. The distortion at the larger pitches of $4D$ and $5D$ is a result of the front being sloped forward at the upper fibers—this sloping is in a direction opposite to that when $S_C \leqslant 2.5D$; as the front approaches an upper fiber, it is retarded by the preceding lower fiber, resulting in this distortion. It is thus the changes in the thermal field as a result of staggering the fibers that bring about this variation in the front behavior with pitch and transverse spacing. As the pitch and transverse spacing are increased, the thermal distortions interact less, and the front propagation returns to planar.

With staggered copper fibers, the distortions in the thermal field induced by the fibers are more localized than for alumina fibers; thus it would be expected that for copper fibers, the staggered fibers would more closely follow the in-line behavior. This is borne out by the results. For the three largest transverse spacings investigated ($H = 2.5$, 3, and $3.5D$), the front progression was identical to that with the in-line fibers, with the front propagation being essentially planar at pitches larger than $S_C = 2D$. For the smaller spacings ($H = 1.5D$ and $2D$), the front undergoes the same "double transition" as for the intermediate spacings investigated for the alumina case: for $H = 2D$ the front is planar at a pitch of $S = 2D$, angled at a pitch of $S = 3D$, and then returns to planar for larger S. For $H = 1.5D$

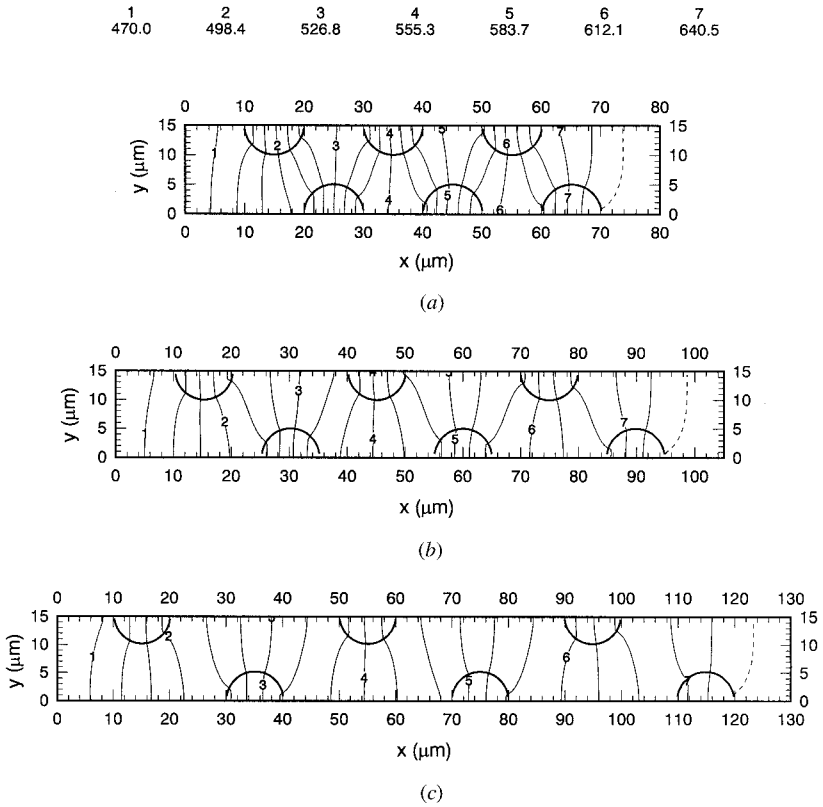

Figure 12. Temperature profiles for aluminum solidification with staggered alumina fibers for the cases considered in Figure 8. Plots are shown at (*a*) 104.5, (*b*) 177.1, and (*c*) 269.5 μs.

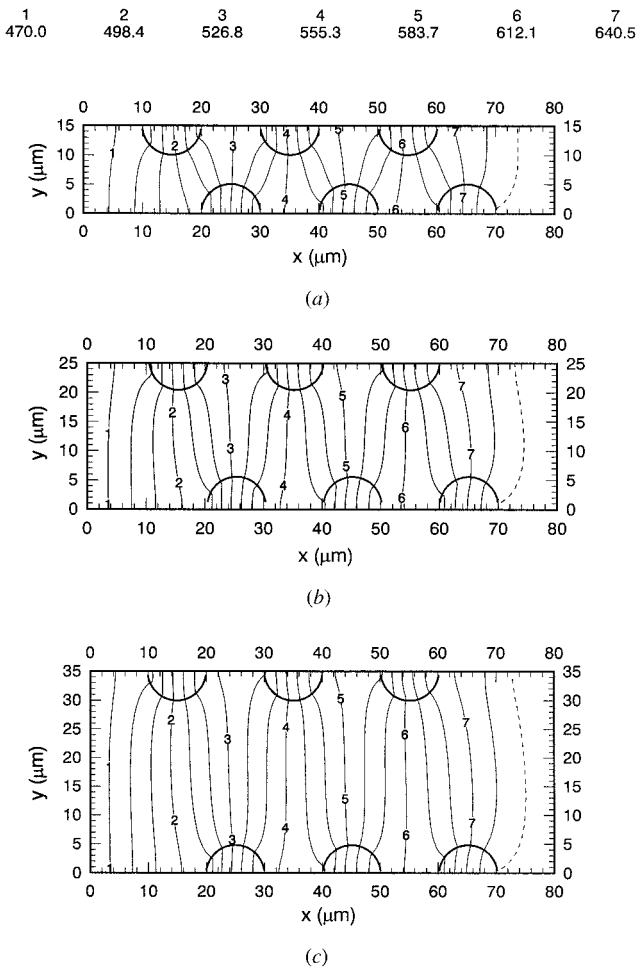

Figure 13. Temperature profiles for aluminum solidification with staggered alumina fibers for the cases considered in Figure 9. Plots are shown at (*a*) 104.5, (*b*) 95.48, and (*c*) 92.40 μs.

the front remains angled at pitches of $S = 2D$ and $3D$, indicating that the transverse spacing is small enough to suppress the first transition.

CONCLUSIONS

Results are presented from a numerical analysis of the solidification of a pure aluminum matrix in the presence of low- and high-conductivity fibers arranged in an in-line or staggered arrangement. Front locations are presented as a function of time, as are thermal fields in the domain. For fibers in an in-line arrangement, a critical pitch S_C was identified: a pitch lower than this critical value causes increasing front distortion with each additional fiber that the front passes, whereas for larger values of pitch, the front has a sufficient distance between fibers in which to return to an essentially planar (vertical) orientation. For alumina fibers the

Table 2. Front orientation for staggered fibers

	S					
H	2D	3D	4D	5D	6D	8D
			Alumina fibers			
1.5D	A	A	A	A	A	A
2D	A	P	A	A	P	P
2.5D	A	P	A	P	P	P
3D	A	P	P	P	P	P
3.5D	A	P	P	P	P	P
			Copper fibers			
1.5D	A	A	P	P	P	P
2D	P	A	P	P	P	P
2.5D	P	P	P	P	P	P
3D	P	P	P	P	P	P
3.5D	P	P	P	P	P	P

A, angled, distorted front incident on fibers; P, essentially planar front incident on successive fibers.

critical pitch was approximately $S_C = 2.5D$, while for copper fibers it was $S_C = 2D$. For fiber spacings smaller than the critical pitch, the fibers may be pushed out of alignment by the (increasingly) distorted front, resulting in a nonuniform dispersion of fibers and final properties.

For staggered fibers, the behavior of the propagating front is more complex and is a result of the interacting thermal distortions of neighboring fibers. For alumina fibers, the front does not return to planar from distorted at any of the pitches tested, at small transverse spacings. Thus there is a critical transverse spacing below which the final properties of the composite are expected to be adversely affected, irrespective of the fiber pitch S. At intermediate transverse spacings, the thermal fields interact only at small fiber pitch; this causes the front progression to lapse from being planar at pitches just larger than the critical spacing, to being angled, and eventually, to being planar once again, once the pitch is increased sufficiently. At larger transverse spacings, the propagation of the front becomes similar to the in-line arrangement; the uniformity and quality of the final material properties would therefore deteriorate for pitches less than S_C. For staggered copper fibers, the thermal distortions around each fiber are less pronounced than for alumina, and the effect of fiber staggering on the front propagation is less pronounced.

The overall solidification time for the system is also affected by the thermal properties of the fibers. In addition, higher fiber thermal conductivities have a stabilizing effect on temperature profiles, while lower conductivities distort temperature profiles long after solidification has occurred.

REFERENCES

1. A. Mortensen, L. J. Masur, J. A. Cornie, and M. C. Flemings, Infiltration of Fibrous Preforms by a Pure Metal: Part 1, Theory, *Met. Trans.*, vol. 20A, pp. 2535–2547, 1989.

2. L. J. Masur, A. Mortensen, J. A. Cornie, and M. C. Flemings, Infiltration of Fibrous Preforms by a Pure Metal: Part 2, Experiment, *Met. Trans*., vol. 20A, pp. 2549–2557, 1989.
3. A. Mortensen and V. Michaud, Infiltration of Fiber Preforms by a Binary Alloy: Part 1, Theory, *Met. Trans*., vol. 21A, pp. 2059–2072, 1990.
4. M. A. Khan and P. K. Rohatgi, Numerical Solution to a Moving Boundary Problem in a Composite Medium, *Numer. Heat Transfer*, vol. 25, pp. 209–222, 1994.
5. M. A. Khan and P. K. Rohatgi, Numerical Solution to the Solidification of Aluminum in the Presence of Various Fibers, *J. Mater. Sci*., vol. 30, pp. 3711–3719, 1995.
6. J. Fan, R. Gibson, and D. Hageman, Microscopical Study on Heat Transfer and Mushy Zone Evolution in Casting of Metal Matrix Composites, in *Transport Phenomena in Solidification*, ASME HTD-vol. 284, pp. 191–196, 1995.
7. S. V. Garimella and J. E. Simpson, Interface Propagation in the Processing of Metal Matrix Composites, *Microscale Thermophys. Eng*., vol. 2, pp. 173–188, 1998.
8. J. E. Simpson, S. V. Garimella, and M. M. Guslick, Interface Propagation in the Presence of a Fibrous Phase in Alloy Solidification, *Heat Transfer 1998*, vol. 7, pp. 235–240, 1998.
9. R. Barrett, M. Berry, T. F. Chan, J. Demmel, J. M. Donato, J. Dongarra, V. Eijkhout, R. Pozo, C. Romine, and H. Van der Vorst, *Templates for the Solution of Linear Systems: Building Blocks for Iterative Methods*, SIAM, Philadelphia, Pa., 1994.